ANALYTICAL ULTRASONICS FOR STRUCTURAL MATERIALS

David S. Kupperman
Argonne National Laboratory
Argonne, Illinois 60439

The application of ultrasonic velocity and attenuation measurements to characterize the microstructure of structural materials is discussed. Velocity measurements in cast stainless steel are correlated with microstructural variations ranging from equiaxed (elastically isotropic) to columnar (elastically anisotropic) grain structure. The effect of the anisotropic grain structure on the deviation of ultrasonic waves in cast stainless steel is also reported. Field-implementable techniques for distinguishing equiaxed from columnar grain structures in cast stainless steel structural members are presented. The application of ultrasonic velocity measurements to characterize structural ceramics in the green state is also discussed.

INTRODUCTION

The reliability of ultrasonic techniques used in the inspection of structural materials is often limited by the peculiar microstructure of the material. This is the case for cast stainless steel (CSS) and for structural ceramics in the "green" (unfired) state. The research described in this paper is directed toward understanding the wave propagation characteristics of these materials so that ultrasonic NDE techniques can be reliably applied to them.

ULTRASONIC CHARACTERIZATION OF CAST STAINLESS STEEL

Background

It is well known that the coarse grain size and elastic anisotropy of CSS make ultrasonic inspection difficult. Although the ASME code requires inspection of CSS piping, it has not been possible to demonstrate that current inspection techniques are adequate. Measures that may increase the reliability of ultrasonic inspection in the near term include (a) the development of methods to establish the microstructure of the material (to help optimize the inspection technique), (b) calibration standards that are more representative of the material to be inspected, and (c) the use of cracked CSS samples for training purposes. For the long term, it will be necessary to establish (a) the variability of the microstructure of CSS, (b) the effect of microstructure on inspection reliability, (c) the degree of improvement possible with techniques and equipment designed specifically for CSS, e.g., focused

*Work funded by the U.S. Nuclear Regulatory Commission, Office of Nuclear Regulatory Research and the U.S. Department of Energy, Advanced Research and Technology Development Fossil Energy Materials Program.

transducers and lower frequencies than those used conventionally, and (d) qualification of requirements for CSS inspections. Recent work carried out at ANL to address some of these points is presented below.

Technical Progress

1. Variation of Sound Velocity with Microstructure

When CSS material is isotropic (composed of equiaxed grains), the variation in velocity with wave propagation direction can be small (<2%), whereas for anisotropic material (composed of columnar grains) the variation in velocity may be large (as much as 100% for shear waves). The magnitude of the sound velocity may also be used as a measure of the degree of anisotropy and thus as an indicator of microstructure. Relatively low longitudinal-wave velocities indicate a columnar grain structure, whereas high velocities may indicate an equiaxed (isotropic) structure. Intermediate values may indicate the presence of both microstructures.

The validity of this concept has been demonstrated on CSS samples with different microstructures. Figure 1 shows the longitudinal-wave velocities for seven 400 x 180 x 60-mm samples of a 28-in. pipe provided by Battelle PNL and 18 samples of a comparable large-diameter pipe provided by Westinghouse. The Battelle samples were fabricated from a weldment in which material with a well-defined equiaxed grain structure was joined to material with a well-defined columnar grain structure. The Westinghouse samples were also made from a weldment. These specimens, however, were machined flat and have a coarse and poorly defined grain structure. Sound velocity was measured by standard pulse-echo methods with a 37-mm-dia, 1-MHz transducer. Echo transit times were measured with a Tektronix oscilloscope. In all cases the longitudinal waves propagate in a radial direction through the pipe wall. As shown in figure 1, the equiaxed and columnar sides of the Battelle samples can be easily distinguished by measurements of the longitudinal-wave velocity. Also, the sample-to-sample variation is relatively small. The Westinghouse samples, however, show large variations in sound velocity from sample to sample as well as within a sample (two measurements were made on each sample). The wide range of the values is indicative of large variations in the microstructure of these samples. This complex microstructure could cause significant, unpredictable distortion of the ultrasonic waves used to interrogate the material and could lead to an unreliable result.

A second set of experiments was performed during a visit to Commonwealth Edison's Byron Station. Sound velocity was measured in the pulse-echo mode in a CSS/carbon steel reference block and two CSS elbows (one each on the steam-generator and pump side of the loop 4 crossover).

On the cast portion of the 7.6-mm-thick reference block, the longitudinal sound velocity was measured at 11 points covering about 0.01 m^2. No significant difficulties were encountered in making these measurements. The average velocity was 6090 m/s, with a variation of about $\pm$1.5% due to the microstructure. The relatively high sound velocity strongly suggests that the reference block has an equiaxed grain structure, which may be significantly different from the grain structure of the plant piping and elbows. As a check on the accuracy of the measurement, the carbon steel portion of the reference block was also examined. A sound velocity of 5890 m/s, which is consistent with previous data for this material, was obtained.

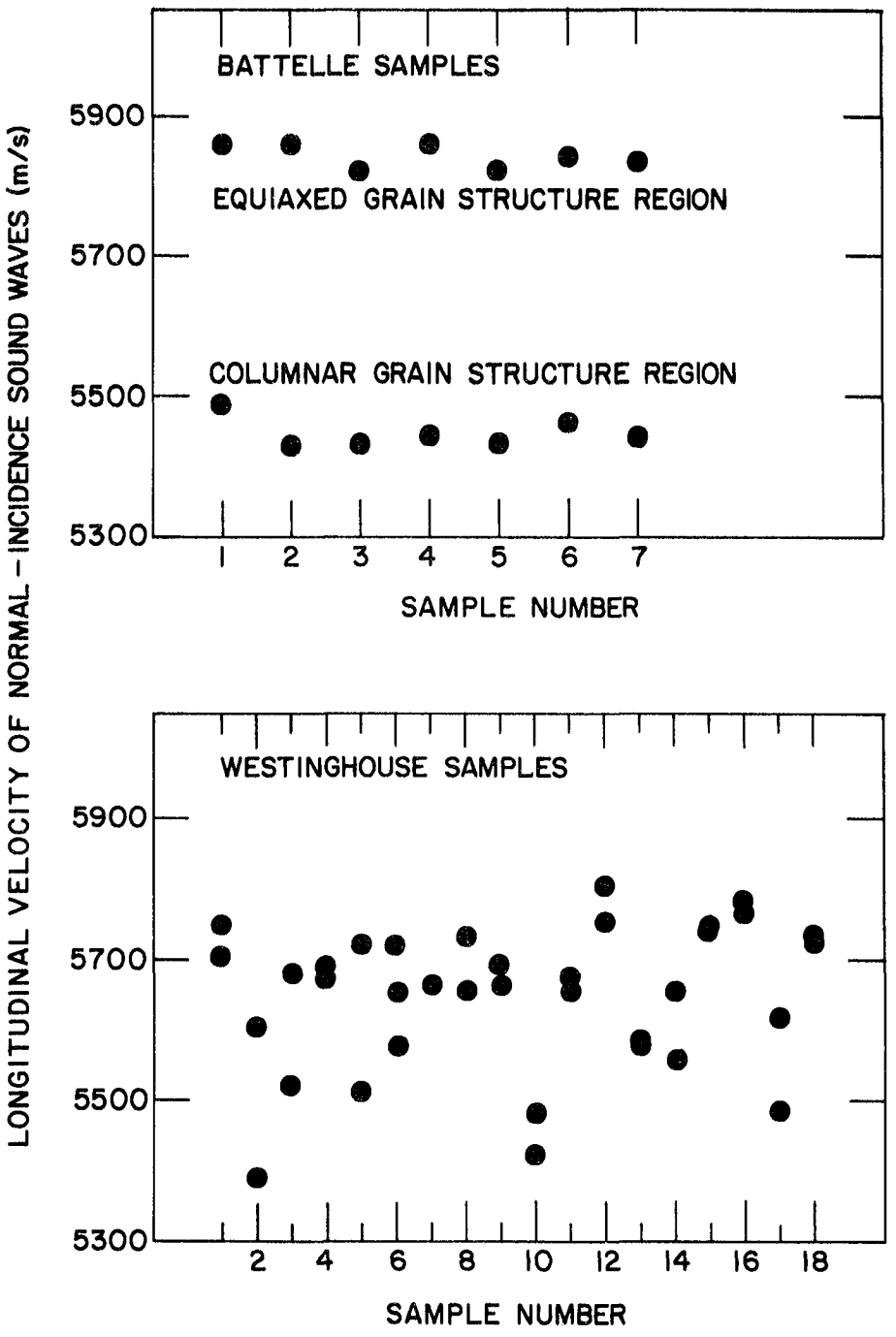

Fig. 1. Variation of Longitudinal-Wave Velocity in Large-Diameter CSS Pipe Sections. (Upper panel) samples with both columnar and equiaxed regions; (lower panel) samples with a poorly defined, coarse grain structure. Two measurements were made on each sample. Sample wall thicknesses are nominally 60 mm; 1-MHz longitudinal waves were propagated normal to the pipe outer surface in a pulse-echo mode.

The surfaces of the CSS elbows were, in most areas, too rough for efficient propagation of ultrasonic waves. Only the smoothly ground areas adjacent to the elbow-to-pipe welds were amenable to pulse-echo examination; ultrasonic backwall echoes could be detected in most, but not all, of these areas. On the pump-side elbow, echoes were detectable at several locations away from the top of the elbow. Since the elbow and pipe appeared to have the same wall thickness, the wall thickness stamped on the pipe section was used as a "best guess" value for the elbow wall thickness. On the basis of this assumption, the sound velocity in the elbow varied from 5200 to 5860 m/s. This suggests that the microstructure of the elbow differed considerably from that of the reference block. The wall thickness of the generator-side elbow could not be estimated because of the elbow geometry, so absolute velocities were not determined; however, the velocity appeared to vary by about 5%. The sound velocity in the straight (wrought) section between the two elbows was found to be 5760 m/s, a value consistent with previous measurements on stainless steel.

Attempts were also made to propagate 1-MHz, 45° longitudinal waves in the cast material with two transducers in a pitch-catch mode. No backwall echo was detected in the reference block; this finding is consistent with the conclusion that the material is equiaxed. No echo signal could be detected on the pump-side elbow, but echoes were present in the generator-side elbow. Thus, the two elbows have distinctly different wave propagation characteristics. However, in both cases there was considerable ultrasonic noise.

These results are consistent with the suppositions that ultrasonic-wave propagation characteristics vary considerably from component to component and within an individual component, and that reference-block material may not be representative of the material to be inspected.

2. Microstructure and Deviation of Ultrasonic Beams

In an elastically isotropic material (composed of equiaxed grains), the energy in an ultrasonic beam propagates in the direction of the wavefront normal, as expected. However, in elastically anisotropic material (with columnar grain structure), the direction of propagation of ultrasonic energy in a beam can be different from the direction of the wavefront normal. Because of this phenomenon, it may be possible to distinguish columnar from equiaxed grain structures nondestructively by examining the propagation behavior of 45° shear or longitudinal waves in the material. Figure 2 shows the predicted shear-wave propagation behavior in 60-mm-thick specimens. For an equiaxed specimen with the transmitter and receiver placed on opposite sides (fig. 2a), the maximum acoustic signal will be detected $\sim$60 mm from the point directly opposite the beam entry point. For a specimen with columnar grains (fig. 2b), the energy in the beam deviates markedly from the expected 45° path, such that the maximum signal will be detected at only $\sim$16 mm (see analysis below) from the point opposite the beam entry point. As shown in figure 2c, the beam in the equiaxed material will be reflected to a point $\sim$120 mm from the transmitting transducer (following the expected "full-V" path), while the maximum reflected-beam intensity in the columnar material will be found much closer to the transmitting transducer ($\sim$32 mm away).

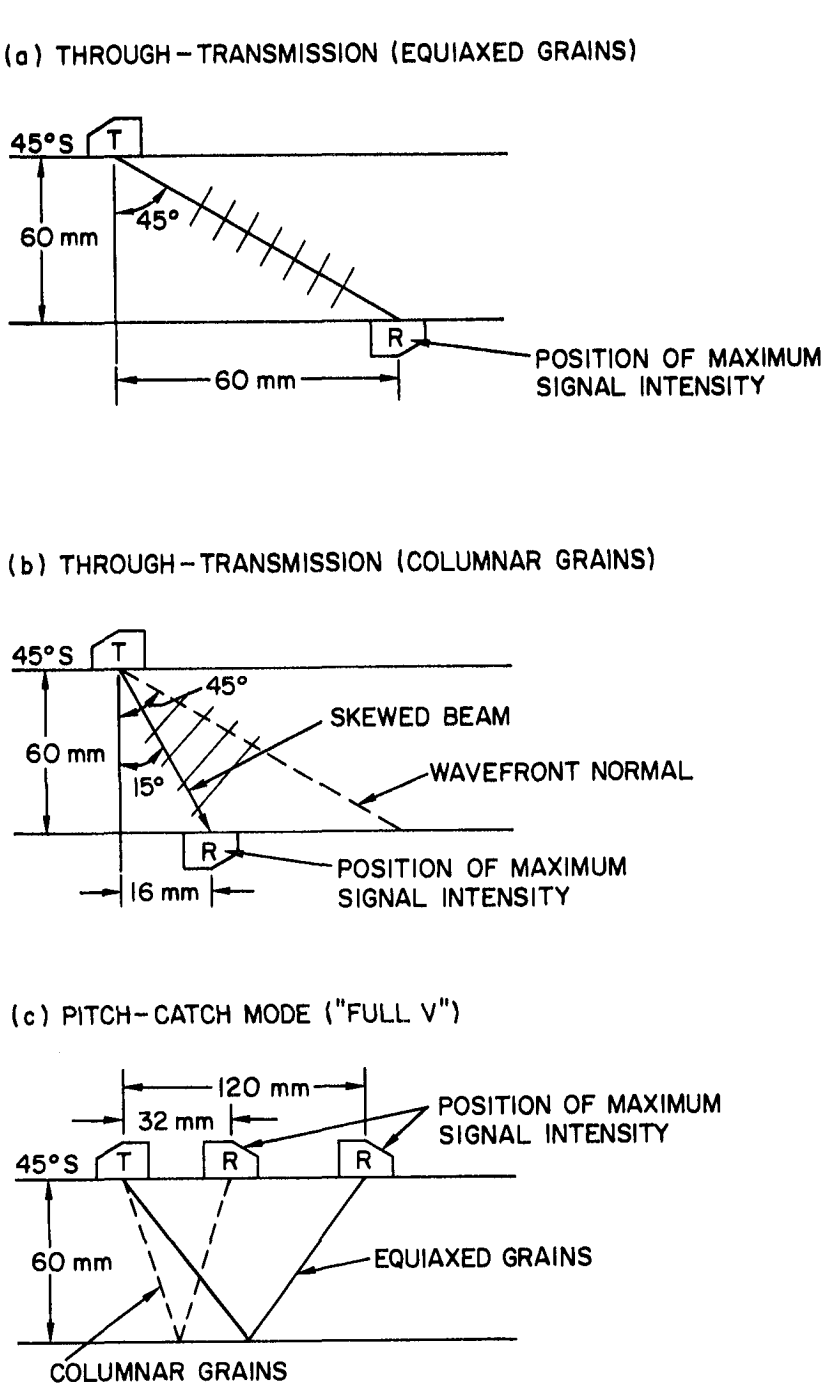

Fig. 2. Schematic Representation of the Path of Ultrasonic Energy in Cast Stainless Steel with Equiaxed vs Columnar Grain Structure. (a) Transmit from outer surface and receive at inner surface (equiaxed grains), (b) transmit from outer surface and receive at inner surface (columnar grains), and (c) transmit and receive at outer surface.

The analysis leading to this prediction is given below. If the angular deviation of longitudinal waves as a function of propagation angle (angle of refraction, in this case) is known, the point of maximum signal intensity for the pitch-catch configuration of figure 2 can be calculated from Snell's law:

$$\frac{\sin \theta_w}{V_w} = \frac{\sin \theta_{CSS}}{V_{CSS}(\theta)} , \tag{1}$$

where θ_w and V_w are the angle of incidence and the velocity, respectively, of the sound wave in the wedge, and θ_{CSS} and V_{CSS} are the angle of refraction and longitudinal velocity of sound in the cast stainless steel. In the case shown, $\sin \theta_w / V_w = 0.22$.

The angular dependence of the velocity of sound must be known in order to calculate the angle of refraction. The orthotropic elastic constants for the columnar-grain CSS were calculated from velocity measurements in two different directions (ref. 1) by use of the Christoffel equations. These constants were then used to calculate the velocity as a function of the angle of incidence, and hence, to calculate the angle of refraction from equation (1). For the wedge used in the velocity measurements, the calculated angles of refraction are 36° for the columnar-grain CSS and nearly 45° for the equiaxed material. The angle between the velocity vector and the direction of maximum energy propagation is 21° for CSS. Hence, the energy of the beam propagates in a direction inclined 15° (i.e., 36° - 21°) to the surface normal, and in a 60-mm-thick sample, the reflected wave should have a maximum signal intensity at the transmitting surface ∿32 mm from the transmitting probe. In the case of the equiaxed specimen, the calculated separation distance for maximum signal intensity is ∿127 mm (the angle of refraction is actually 47°; hence, the calculated separation distance is slightly larger than the value of 120 mm expected for a 45° angle).

To verify these predictions, experiments were carried out on one columnar and one equiaxed pipe region from a sample similar to the Battelle pipe sections mentioned earlier. Two 0.5-MHz, nominally 45° shear-wave transducers (25 x 25 mm in size) were placed on the outer surface of each pipe section, and the separation between the two transducers was varied to maximize the received signal. Table I compares the optimum separations determined in these experiments with the corresponding predicted values. The agreement is reasonable.

Table I. Transducer Pair Separation[a] for Maximum Received Signal on Outer Surface of 60-mm-Thick CSS Pipe Sections

Grain Structure	Predicted Value, mm	Measured Value, mm
Columnar	32	42
Equiaxed	127	105

[a]45° shear waves in pitch-catch "full-V" configuration at 0.5 MHz.

3. Visualization of Ultrasonic Beam Distortion

The distortion of an ultrasonic beam as it propagates through weld metal can be visualized by use of a beam profile analyzer (courtesy of Sonoscan, Inc., Bensenville, IL). Figure 3 shows the schematic arrangement of this commercially available device. A transducer and sample are placed in a water bath. The ultrasonic beam (pulsed) travels through the specimen and strikes a gold-plated plastic plate. A laser beam scans the gold film and, by use of an optical interferometer, monitors the intensity of the beam in the plane of the film. The light-beam spot is 250 μm across and has a field coverage of 10 x 10 cm. The oscilloscope images discussed below were produced with a 1-cm-dia (2.25 MHz) transducer; the gain of the system was adjusted to make the maximum detected intensity of the ultrasonic beam the same in all cases.

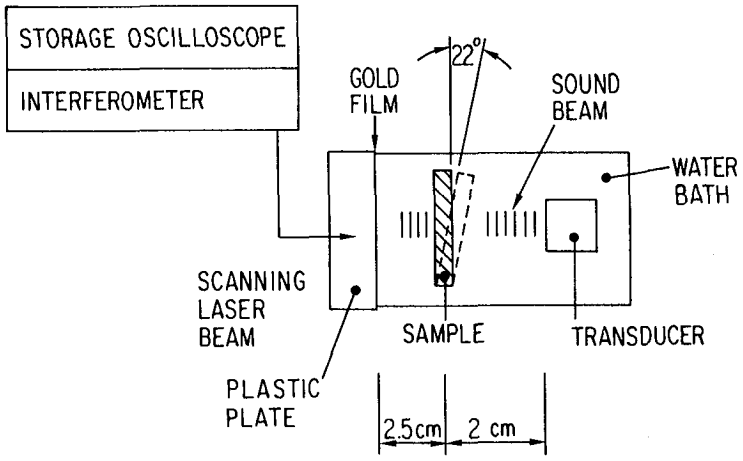

Fig. 3. Schematic Arrangement of Beam Profile Analyzer with Ultrasonic Beam Passing through Weld-Metal Sample.

Longitudinal waves are expected to converge when propagating along a direction 45° to the grain axis in columnar CSS or SS weld metal. Figures 4a and b show the images produced by identical 2.25-MHz longitudinal waves traveling through water alone and through 12 mm of weld metal at 45° to the grain axis, respectively. In the latter case, the incident ultrasonic beam was normal to the specimen surface. Despite the short path, the beam was distorted as it passed through the weld metal, with focusing of the beam in the horizontal (110) plane, but not in the orthogonal plane. The difference in the way the velocities vary with propagation direction accounts qualitatively for the elliptical shape of the beam emerging from the specimen.

Figures 4c and d show the ultrasonic beam distortion produced for longitudinal waves propagating parallel and perpendicular, respectively, to the columnar grains. Again, the incident beam was normal to the specimen surface. In both cases, the emerging beam was weak relative to the one propagated at 45° to the grains (fig. 4b), and was distorted more in the horizontal plane than the vertical. Figure 4e shows the cross section of a beam propagated through a 4-mm-thick slice from a weld-metal specimen, at an angle of incidence of about 22°. With this sample orientation,

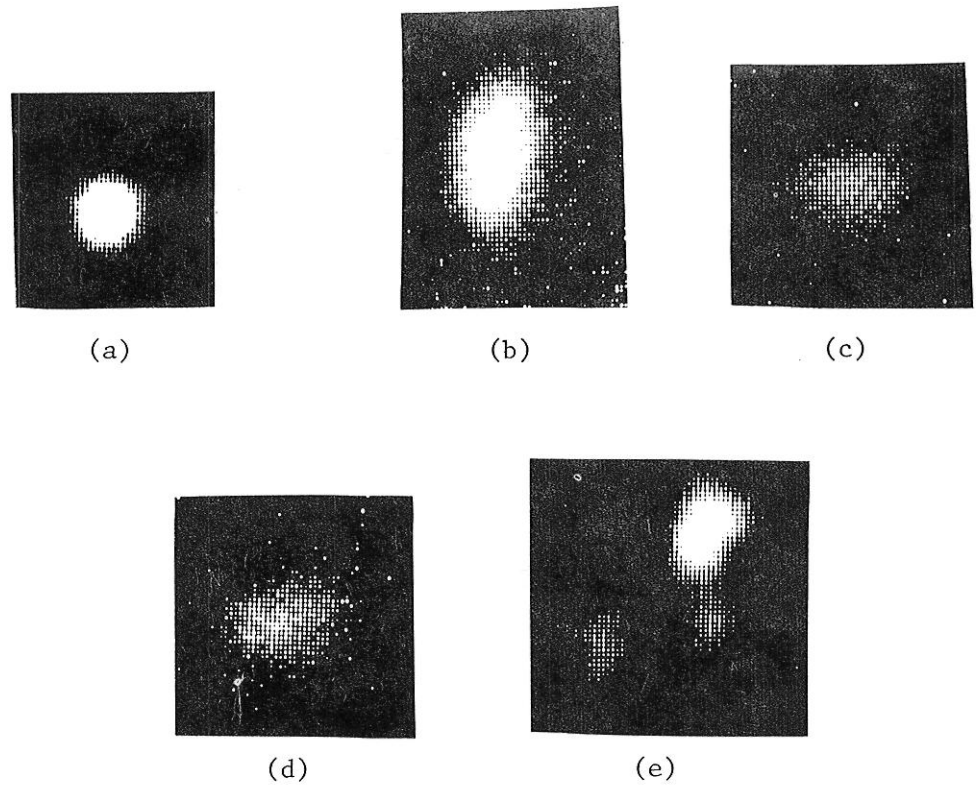

Fig. 4. Cross Section of Longitudinal Beam Passing through (a) Water; (b-e) Weld Metal Oriented with the Grain Axis (b) at 45° to the Beam Axis; (c) Parallel to the Beam Axis; (d) Perpendicular to the Beam Axis; and (e) at an Angle That Allows Only Shear Waves to Travel through the Weld Metal.

longitudinal waves were mode converted to shear waves which then propagated approximately perpendicular to the columnar grain axes. (The shear waves mode-converted back to longitudinal waves in the water.) In this case, the propagation in weld metal produced a large, nonuniform distortion. In contrast, a beam propagated through a similar sample of isotropic metal emerged from the sample with a highly uniform cross section (data not shown). This effort demonstrates that visualization of ultrasonic beams can lead to better insight into the distortion of ultrasonic waves as they pass through transverse isotropic material.

ULTRASONIC CHARACTERIZATION OF GREEN CERAMICS

Background

Development of NDE methods for green (unfired) ceramics could result in considerable cost savings in fabricating structural components, as the final firing stage would be eliminated for defective components. This section describes a preliminary investigation to study the propagation of ultrasonic waves in green ceramics

and to assess the potential of ultrasonic NDE methods as a source of useful quantitative information on defects, cracking, delaminations, agglomerates, inclusions, regions of high porosity, and anisotropy.

The difficulties associated with ultrasonic examination of green ceramics are formidable. For example, low-frequency sound waves are not scattered sufficiently to allow the detection of flaws much smaller than 1 mm in size; on the other hand, sound waves with frequencies of $\gtrsim$3 MHz generally undergo excessive attenuation in samples >3 mm thick. Also, ordinary couplants (e.g., water or glycerol) are often absorbed by green ceramics; this not only mitigates their coupling function, but may also affect the subsequent fabrication process. This problem can be avoided by using pressure alone to couple the transducer to the specimen, but great care is required because the applied pressure can affect the measured velocity and attenuation, particularly for high-frequency longitudinal waves, or even result in breakage of the fragile specimen.

In spite of these difficulties, studies of ultrasonic attenuation and acoustic velocity (including dispersion and frequency spectra) in green ceramics may provide useful information related to density variations, porosity content, presence of agglomerates and delaminations, elastic anisotropy, and material quality in general; some examples of promising approaches are presented below. Further development of ultrasonic testing techniques, coupled with signal enhancement techniques, may lead to improved flaw detection sensitivity.

Technical Progress

Green ceramic specimens were provided by the Ceramics Group of the Materials Science and Technology Division at Argonne National Laboratory (ANL) and the Materials Chemistry Division of the National Bureau of Standards (NBS). The specimens were generally 50-60% of theoretical density and very fragile. The main experimental effort was carried out with silicon nitride disks 3.3 cm in diameter and 0.6 cm thick and magnesium aluminate spinel disks 3.7 cm in diameter and 0.6 cm thick. Some other materials were also included. The specimens were cold pressed with various loading pressures and additions of polyvinyl alcohol (PVA) or Carbowax (CW) binder.

1. Elastic Anisotropy

The elastic anisotropy of a green ceramic specimen can be determined from the change in sound velocity that occurs when a shear-wave transducer is rotated with respect to the specimen, thus varying the polarization of the shear waves propagating in a particular direction. Sound velocity data were acquired for Si_3N_4, $MgAl_2O_4$, MgO, and $YCrO_3$ specimens with a Panametric 5052UAX ultrasonic transducer analyzer and a Tektronix 7904 oscilloscope with 7B85 and 7B80 time bases. Panametric 2.25-MHz normal-incidence shear-wave transducers (13 mm in diameter) and Aerotech 2.25-MHz alpha transducers (6 mm in diameter) were employed for the measurements. The velocity was measured by overlapping successive echoes in the pulse-echo mode and determining the time delay from the oscilloscope. The time base was calibrated by checking the oscilloscope readings against a sequence of precisely timed pulses from a Tektronix type 184 time mark generator. With the MgO specimens, which have a

high content of CW binder, Panametric shear-wave couplant was successfully used for both longitudinal and shear waves. With the chalk-like $YCrO_3$ specimens (<1% PVA binder), no couplant was needed for either type of wave.

Figure 5 shows the echo pattern for 2.25-MHz longitudinal and shear waves in a 3.8-mm-thick $YCrO_3$ specimen. (About 6 μs separate the first and second longitudinal echoes; about 10 μs separate the shear echoes.) Apparent attenuation is clearly rather high, on the order of 10-20 dB/cm. Furthermore, the effect of polarization on shear-wave velocity shows that the material is elastically anisotropic: A maximum velocity variation of about 3% was reproducibly observed as the shear-wave transducer was rotated about its axis while remaining over the same point on the sample. (The pressure of the transducer on the sample was controlled so that the velocity variations could not be attributed to variations in transducer loading.) Table II summarizes the sound velocity data for the $YCrO_3$ sample. The low value of Poisson's ratio implies that under stress, the volume of the specimen is significantly reduced; this is consistent with the porous, low-density nature of the sample. Since the modulus of elasticity is related to the velocity of sound, variations in shear velocity with polarization can indicate variations of modulus with direction. This variation in modulus could affect the performance of a component made from such a sample.

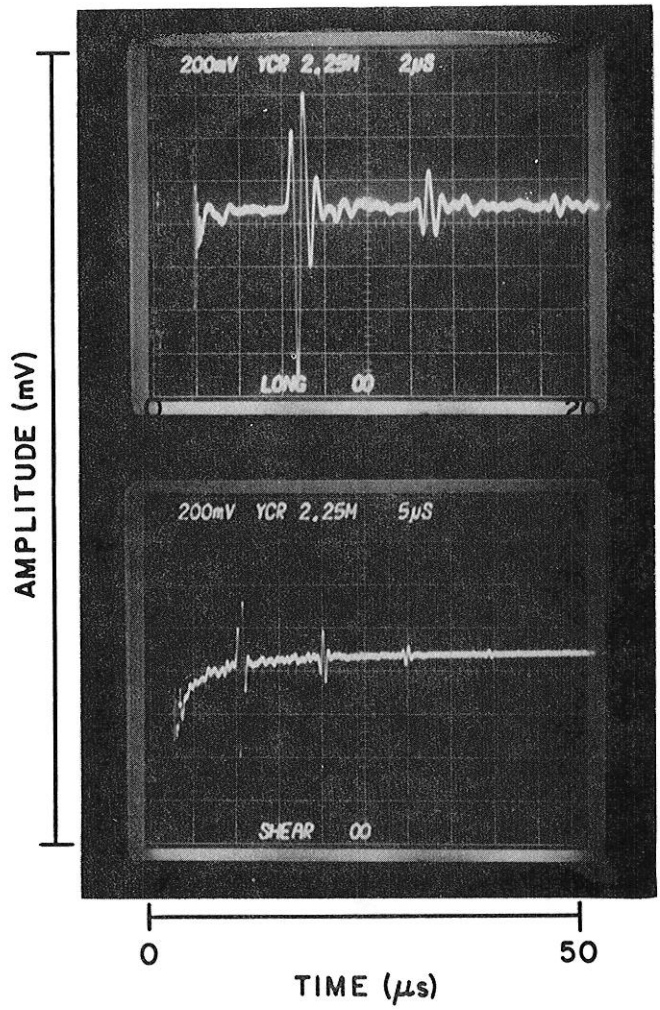

Fig. 5. Echoes from a 3.8-mm-Thick $YCrO_3$ Sample Insonified with (Top) Longitudinal Waves and (Bottom) Shear Waves at 2.25 MHz. Axis dimensions are as follows: Ordinate - 200 mV/div.; abscissa - 2 μs/div. in upper panel, 5 μs/div. in lower panel.

Table II. Sound Velocity in $YCrO_3$ Sample with PVA Binder

Longitudinal Velocity (10^5 cm/s)	Shear Velocity (10^5 cm/s)	Poisson's Ratio, σ
1.43	0.947 max	0.11
1.43	0.919 min	0.15

Another example of variation with polarization was observed in a 3-mm-thick section of a spinel disk, insonified with shear waves propagating in the plane of the disk. With polarization parallel to the disk axis, the velocity (error <0.5%) was about 3.5% higher than with polarization perpendicular to the disk axis. No variation of velocity with polarization was found for wave propagation parallel to the disk axis. This implies that the shear modulus is greatest in the pressing direction.

2. Variation of Velocity with Density

The velocity of longitudinal waves has been measured as a function of density for MgO specimens with 20 wt.% CW binder. Density variations among these specimens result from differences in loading pressure, i.e., in porosity. Figure 6 shows a plot of density vs sound velocity for four samples. One of the samples is anomalous (it has a visible delamination). From the results for the other three samples, a linear relationship between velocity and density is apparent; the variation in density is 1/3 the variation in velocity. Also shown in figure 6 is the nominal variation in density for three of the samples (rectangles around the data points), determined from variations in velocity measurements taken at five different points on each sample. Variations in density of up to 2% were observed. These results suggest that not only can the density (and thus porosity) of a sample be determined from sound velocity measurements, but if sufficiently small transducers were available, anomalous microstructures could be detected by mapping local variations in density.

The maximum density (0% porosity) of MgO-20 wt.% CW, calculated from the densities of the two constituents, is 2.7 g/cm^3. The velocity obtained at this density by extrapolating the curve of figure 6 is 8.1×10^5 cm/s. This velocity can be compared to theoretical models that predict upper and lower bounds for sound velocity in a homogeneous composite material with a soft matrix and hard filler, as a function of the volume fraction of one of the constituents. Theoretical values for the longitudinal velocity were calculated as a function of volume fraction by using both the Voigt model (which assumes constant strain and gives an upper bound for velocity) and the Reuss model (which assumes constant stress and gives a lower bound). The velocities were calculated according to the following relationships (ref. 2):

$$\rho v_{\ell_v}^2 = f_1 \rho_1 v_{\ell_1}^2 + f_2 \rho_2 v_{\ell_2}^2 \quad \text{(Voigt velocity)}, \tag{2}$$

$$\frac{1}{\rho v_{\ell R}^2} = \frac{f_1}{\rho_1 v_{\ell_1}^2} + \frac{f_2}{\rho_2 v_{\ell_2}^2} \quad \text{(Reuss velocity)}, \tag{3}$$

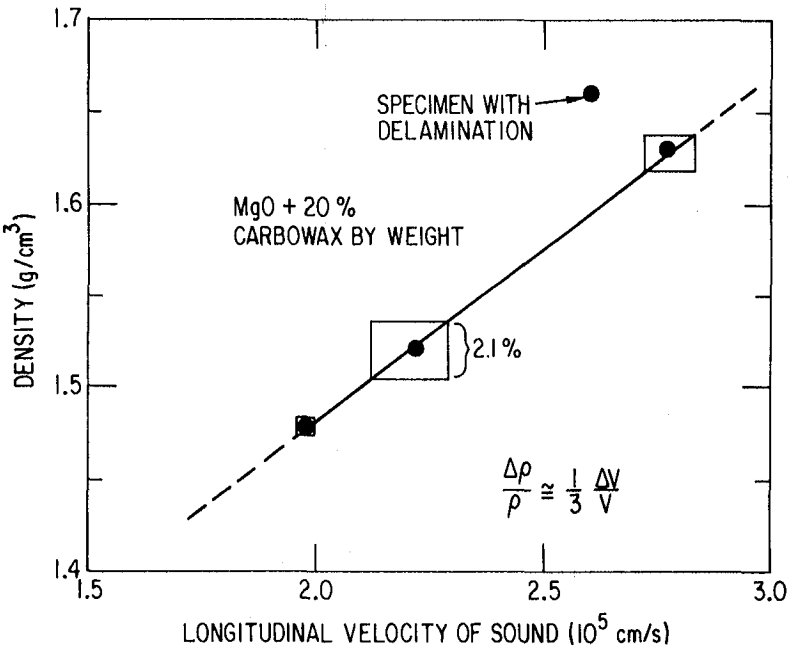

Fig. 6. Sample Density vs Longitudinal Velocity of Sound for MgO + 20% Carbowax. Rectangles show variation within each sample.

where f_1, f_2 are fractional volumes, ρ_1, ρ_2 are densities, and v_{ℓ_1}, v_{ℓ_2} are longitudinal velocities for constituents 1 and 2, respectively, and $\rho = f_1\rho_1 + f_2\rho_2$. Figure 7 shows the resultant upper (Voigt) and lower (Reuss) velocity limits for MgO/CW composites vs the volume fraction of CW. The extrapolated velocity for a volume fraction of 37.5% CW (the amount used in the ANL pellets) is indicated. This value is within the theoretical bounds and is close to the Voigt limit.

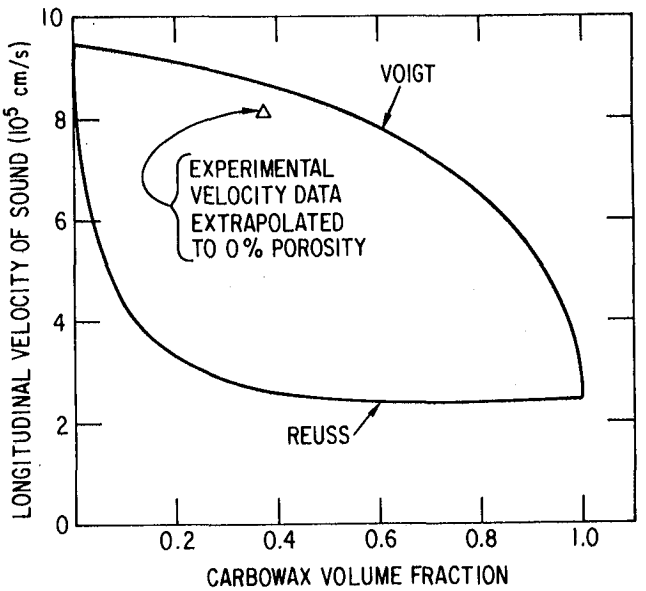

Fig. 7. Theoretical Upper and Lower Bounds for Longitudinal Velocity vs Carbowax Volume Fraction. Experimental value determined from extrapolation of data in Fig. 6 is also shown.

These results indicate that sound velocity measurements can provide quantitative information on porosity and local fluctuation in density, and can perhaps indicate anomalous microstructures. The analysis also indicates that data acquired in this manner may be predicted by models for composites, further suggesting that sound velocity data and relationships to anomalous microstructures may be understood from a fundamental point of view.

REFERENCES

1. Kupperman, D. S.; Reimann, K. J.; and Kim, D. I.: Ultrasonic Characterization and Microstructure of Stainless Steel Weld Metal. Nondestructive Evaluation: Microstructural Characterization and Reliability Strategies, O. Buck and S. M. Wolf, Eds., The Metallurgical Society of AIME, 1981, pp. 191-216.

2. Lees, S. and Davidson, C. L.: Ultrasonic Measurement of Some Mineral Filled Plastics, IEEE Trans. Sonics Ultrason. SU-24(3), 222 (May 1977).